Benzoylpivaloylmethanide Precursors for the Chemical Beam Epitaxy of Oxide Thin Films. 1. Synthesis, Characterization, and Use of Yttrium Benzoylpivaloylmethanide

E. Fritsch,[†] E. Mächler,[‡] F. Arrouy,[†,‡] O. Orama,[§] H. Berke,[†] I. Povey,[⊥] P. R. Willmott,[⊥] and J.-P. Locquet*[,‡]

Institute of Inorganic Chemistry, University of Zurich, 8057 Zurich, Switzerland; IBM Research Division, Zurich Research Laboratory, 8803 Rüschlikon, Switzerland; V. T. T. Chemical Technology, 02044 VTT, Finland; and Institute of Physical Chemistry, University of Zurich, 8057 Zurich, Switzerland

Received April 25, 1996. Revised Manuscript Received September 6, 1996[⊗]

The new complex yttrium benzoylpivaloylmethanide and its acetonitrile adduct have been characterized by IR, NMR, mass spectroscopy, X-ray structure analysis, and thermogravimetric/differential thermal analysis. In situ flux measurements and mass spectroscopic studies have been performed to test the suitability of this compound as a precursor for the deposition of complex oxide thin films under molecular beam conditions. Finally it has been used to deposit epitaxial Y_2O_3 (001) thin films on $SrTiO_3$ (001) substrates.

Introduction

Chemical vapor deposition techniques under ultrahigh-vacuum (UHV) conditions have attracted considerable attention owing to an increased demand for customized and well-defined thin films of high purity with precisely controlled properties.[1] Chemical beam epitaxy (CBE) operates under nearly the same vacuum conditions as molecular beam epitaxy (MBE) but uses metalorganic precursors to transport the desired atomic species to the substrate. It offers a multitude of advantages over conventional low-vacuum physical (PVD) and metalorganic (MOCVD) vapor deposition methods: (1) substrates can be cleaned and characterized in situ before deposition; (2) vapor-phase molecular interactions and reactions can be minimized owing to the reduced molecular mean free path; (3) growth can be controlled in situ using surface characterization techniques such as reflection high-energy electron diffraction (RHEED), photoemission spectroscopy (XPS), and Auger electron spectroscopy; (4) ultrathin films and sharp substrate/film interfaces can be obtained; (5) it is possible to decrease the deposition temperatures because electron or ion beams can help activate the growth process.[1,2] The advantages of CBE over MBE are (1) the higher volatility of the metalorganic precursors, which allows using lower effusion-cell temperatures for similar deposition rates, (2) the improved oxidation resistance of the precursors (elementary barium and lanthanum sources, e.g., are very sensitive toward oxygen), (3) the simpler and less expensive equipment (no electron beam evaporators are needed), and (4) the potential to chemically influence the growth process by, for instance, an increased surface diffusion. The main disadvantages of the CBE technique are (1) the generally slow deposition rate, (2) the expensiveness of the equipment, and (3) the difficulties associated with large-area deposition and uniformity.

We have developed a CBE approach using Knudsen effusion cells for the deposition of oxide thin films.[3−5] This method requires the design of novel precursors, as the compounds conventionally used for the preparation of oxides by MOCVD techniques are not tuned for efficient use under molecular beam conditions. Their high volatility and low sticking coefficients render sequential deposition techniques difficult.[6] The *ideal* precursor for our CBE purposes will meet the following requirements: (1) a very low background pressure ($\simeq 10^{-8}$ Torr) at a rate of 1−10 Å/s; (2) a single metal-containing volatile species in the molecular beam (for accurate in situ flux measurements); (3) a high sticking coefficient ($\simeq 1$) on the cell shutter and system walls; (4) high long-term stability at the evaporation temperature (no decomposition or oxidation of the source material); (5) low toxicity and simple maintenance under atmospheric conditions. Here we report the properties of yttrium benzoylpivaloylmethanide ($Y(bpm)_3$), tested against the above requirements, and describe its use for the preparation of yttria thin films. This paper is the first in a series on the use of alternative β-diketonate precursors for oxide thin-film deposition by CBE.

[†] Institute of Inorganic Chemistry, University of Zurich.
[‡] IBM Zurich Research Laboratory.
[§] V. T. T. Chemical Technology.
[⊥] Institute of Physical Chemistry, University of Zurich.
[⊗] Abstract published in *Advance ACS Abstracts,* October 15, 1996.

(1) Carlsson, J.-O.; Jansson, U. *Prog. Solid State Chem.* **1993**, *22*, 237.
(2) (a) Proc. IV. Int. Conf. CBE Related Growth Techniques. *J. Cryst. Growth* **1994**, *136*. (b) Jones, A. C. *Adv. Mater.* **1993**, *5*, 81. (c) Heinecke, H. *Physica Scripta* **1993**, *T49*, 742. (d) Hamm, R. A.; Ritter, D.; Temkin, H. *J. Vac. Sci. Technol.* **1994**, *A12*, 2790.
(3) Locquet, J.-P.; Mächler, E., manuscript in preparation.
(4) Willmott, P. R.; Felder, P.; Lingenauer, M.; Huber, J. R.; Fritsch, E.; Bidell, W.; Berke, H.; Mächler, E.; Williams, E. J.; Locquet, J.-P.; Bednorz, J. G. *J. Vac. Sci. Technol. A* **1995**, *13*, 248.
(5) Mächler, E.; Locquet, J.-P.; Fritsch, E.; Williams, E. J.; Willmott, P.; Lingenauer, M.; Felder, P.; Huber, J. R.; Berke, H. *Physica C* **1994**, *235*, 705.
(6) Endo, K.; Saya, S.; Misawa, S.; Yoshida, S. *Thin Solid Films* **1991**, *206*, 143.

S0897-4756(96)00251-7 CCC: $14.00

Results on the use of lanthanum benzoylpivaloylmethanide will be discussed in a subsequent report.[7]

Owing to their high values of electric resistivity, good transparency in a wide spectral range and stability against radiation and high temperature, yttria thin films are well suited for a wide range of applications. They are used as interference filters for UV-laser applications,[8] as optical[9] and protective coatings,[10,11] as dielectric layers in multilevel integrated circuits,[12,13] and as electroluminescent devices.[14] Moreover, Y_2O_3 (as well as the isostructural Dy_2O_3[15]) is attractive as a buffer layer for the deposition of $YBa_2Cu_3O_{7-x}$ thin films[16,17] and has been used in sandwich structures to demonstrate Josephson supercurrents[18] and to measure tunneling characteristics.[19] A common method for the deposition of yttrium oxide films is electron beam evaporation,[11,12] but in the past years also MOCVD has been used quite extensively;[10,13,20,21] other techniques include MBE,[22] rf sputtering,[14] laser ablation,[23] and atomic layer epitaxy.[24] To our knowledge, there has so far been only one report that describes the deposition of Y_2O_3 by CBE.[25] Among the various precursors used for chemical vapor deposition of yttrium oxide (for an overview see ref 24), yttrium 2,2,6,6-tetramethylheptanedionate ($Y(thd)_3$) is by far the most important. Although it has been successfully applied for the preparation of Y_2O_3 and $YBa_2Cu_3O_{7-x}$ by CBE,[6,25] it does not fulfill our requirements for a CBE precursor, mainly because of its high volatility. As shown by thermogravimetric studies,[26,27] the simplest method to decrease the volatility (and to increase the sticking coefficient) of a β-diketonate complex is the substitution of alkyl for aryl substituents in the ligand. In the case of yttrium, the complexes with benzoylacetone and dibenzoylmethane do not have a sufficient thermal stability to be sublimed without decomposition under vacuum. The anhydrous acetylacetonate complex $[Y(acac)_3]_n$,[28] on the other hand, is too volatile and forms oligomers in the gas phase. The yttrium complex with 1-phenyl-4,4-dimethyl-3,5-pentanedione (benzoylpivalyolmethane), however, has proven to be suitable for our purposes.

Experimental Section

Fourier transform infrared (FTIR) spectra were obtained as Nujol mulls between NaCl plates on a Biorad FTS-45 instrument. ^1H and ^{13}C NMR spectra were recorded on a Varian Gemini 300 operating at 300 MHz (solvent: acetone-d_6, δ in ppm relative to tetramethylsilane). Preliminary thermogravimetric analyses were made using a Perkin-Elmer TGA 7 thermobalance connected to a TAC 7 processor. Combined thermogravimetric (TGA) and differential thermal analyses (DTA) were performed on a Mettler 2000 C system. About 25 mg of the complex was weighed into an alumina crucible closed by a lid and heated under oxygen or nitrogen (30 mL/min) at a rate of 5 °C/min. The ex situ electron ionization and chemical ionization mass spectra were obtained with a Finigan Mat 8430 mass spectrometer.

The recordings of the electron ionization mass spectra during the precursor beam characterization and in situ thin-film growth were obtained using a Hiden 2000 mass spectrometer. The instrument can measure up to 1000 amu and is equipped with a cross-beam ion source that allows the beam to be sampled without contamination from the ion-source walls.

The experimental system used for precursor beam studies in the Department of Physical Chemistry of the University of Zurich has been described and shown schematically elsewhere.[4] For experiments to determine the thermal decomposition products, a resistively heated substrate holder is mounted downstream from the chopper wheel at 45° to the beam axis, and the QMS (Balzers QMA 150) is placed at 90° to the beam axis. Decomposition spectra were recorded by observing the fragments resulting from impingement of a beam of $Y(bpm)_3$ on a heated MgO substrate at 320, 400, and 510 °C.

Synthesis and Chemical Characterization of $Y(bpm)_3 \cdot CH_3CN$ and $Y(bpm)_3$. Benzoylpivaloylmethane (Hbpm) ligand was prepared according to a literature procedure.[31] Yield 89%, bp 93−95 °C/10^{-2} atm. IR (in substance, range 1700−400 cm^{-1}) 1603 strong (s), 1572 (s), 1481 medium (m), 1463 (s), 1364 (m), 1286 (s), 1239 weak (w), 1183 (w), 1131 (w), 1078 (m), 1028 (w), 930 (w), 848 (m), 768 (s), 695 (s), 652 (w), 569 (w), 490 (w). ^1H NMR (acetone-d_6, δ in ppm) 1.3 (s, 9H), 6.6 (s, 1 H), 7.5−8.1 (m, 5 H). δ (OHO) at the downfield end of the spectrum (≃16−17 ppm) is too broad to be localized. ^{13}C NMR (acetone-d_6, δ in ppm) 27.5 (CH_3, ^{t}Bu), 40.4 ($C(CH_3)_3$), 92.7 (*C*H), 127.7 (Ph, C_{para}), 129.3 (Ph, C_{meta}), 132.9 (Ph, C_{ortho}), 135.9 (Ph, C_{ipso}), 184.8 (PhCO), 204.1 (^{t}BuCO).

Benzoylpivaloylmethane (Hbpm, 15 g, 73.5 mmol) was reacted with 2.94 g (73.5 mmol) of NaOH in 50 mL of EtOH (95%). The yellow solution was added to a solution of 10 g of $Y(NO_3)_3 \cdot 7H_2O$ (25 mmol) in 50 mL of EtOH. A precipitate of $NaNO_3$ formed immediately. After stirring for 3 h at room temperature (RT), water was added, and the oily white product extracted with 3 × 100 mL of pentane. The organic phase was washed with brine and water and dried over Na_2SO_4. Removal of the solvent yielded a white solid, which was dissolved in acetonitrile at RT. Crystals of the acetonitrile adduct appeared after 30 min. They were collected by filtration and dried under vacuum (10^{-1}−10^{-2} atm) at RT. The yield was 74%, melting point 184 °C. Anal. Calcd for $YC_{37}H_{48}NO_6$ compound (MG

(7) Fritsch, E.; Arrouy, F.; Mächler, E.; Locquet, J.-P.; Hubener, R.; Berke, H., manuscript in preparation.
(8) Krakauer, B. W.; Gau, J. S.; Smith, D. J. *J. Mater. Sci. Lett.* **1986**, *5*, 667.
(9) Atanassov, G.; Thielsch, R.; Popov, D. *Thin Solid Films* **1993**, *223*, 288.
(10) Larkin, D. J.; Interrante, L. V.; Bose, A. *J. Mater. Res.* **1990**, *5*, 2706.
(11) Adams, R. O.; Nordin, C. W. *Thin Solid Films* **1987**, *154*, 101.
(12) Basak, D.; Sen, S. K. *Thin Solid Films* **1995**, *254*, 181.
(13) Sharma, R. N.; Rastogi, A. C. *J. Appl. Phys.* **1993**, *74*, 6691.
(14) Cranton, W. M.; Spink, D. M.; Stevens, R.; Thomas, C. B. *Thin Solid Films* **1993**, *226*, 157.
(15) Catana, A.; Locquet, J.-P. *J. Mater. Res.* **1993**, *8*, 1373; *Appl. Surf. Sci.* **1993**, *65/66*, 192.
(16) Edwards, J. A.; Chew, N. G.; Goodyear, S. W.; Satchell, J. S.; Blenkinsop, S. E.; Humphrys, R. G. *J. Less-Common Met.* **1990**, *164*, 414.
(17) Oishi, A.; Teshima, H.; Ohata, K.; Izumi, H.; Kawamoto, S.; Morishita, T.; Tanaka, S. *Appl. Phys. Lett.* **1991**, *59*, 1902.
(18) Blamire, M. G.; Morris, G. W.; Somekh, R. E.; Evetts, J. E. *J. Phys. D* **1987**, *20*, 1330.
(19) Ying, Q. Y.; Hilbert, C.; Kumar, N.; Eichman, D.; Thompson, M.; Kroger, H.; Hwang, D. M. *Appl. Phys. Lett.* **1991**, *59*, 3036.
(20) Varhue, W. J.; Massimo, M.; Carulli, J. M.; Baranauskas, V.; Adams, E.; Broitman, E. *J. Vac. Sci. Technol. A* **1993**, *11*, 1870.
(21) Akiyama, Y.; Sato, T.; Imaishi, N. *J. Cryst. Growth* **1995**, *147*, 130.
(22) (a) Muthe, K. P.; Gupta, M. K.; Gandhi, D. P.; Vyas, J. C.; Kothial, G. P.; Singh, K. D.; Sabharwal, S. C. *J. Cryst. Growth* **1994**, *139*, 323. (b) Vyas, J. C.; Kothial, G. P.; Muthe, K. P.; Gandhi, D. P.; Debnath, A. K.; Sabharwal, S. C.; Gupta, M. K. *Ibid.* **1993**, *130*, 59.
(23) Reisse, G.; Keiper, B.; Weissmantel, S.; Johansen, H.; Scholz, R.; Martini, T. *Thin Solid Films* **1994**, *241*, 119.
(24) Mölsä, H.; Niinistö, L.; Utrianen, M. *Adv. Mater. Opt. Electron.* **1994**, *4*, 389.
(25) Bade, J. P.; Baker, E. A.; Kingon, A. I.; Davis, R. F.; Bachmann, K. J. *J. Vac. Sci. Technol. B* **1990**, *8*, 327.
(26) Ozawa, T. *Thermochim. Acta* **1991**, *174*, 185.
(27) Murray, J. P.; Hill, J. O. *Rev. Inorg. Chem.* **1993**, *13*, 215.
(28) Caulton, K. G.; Streib, W. E.; Coan, P. S. *Inorg. Chem.* **1993**, *32*, 497.
(29) Locquet, J.-P.; Mächler, E. *J. Vac. Sci. Technol. A* **1992**, *10*, 3100.
(30) Vorländer, D.; Kalkow, F. *Ber. Dtsch. Chem. Ges.* **1898**, *30*, 148.
(31) Cornforth, J.; Patrick, V. A.; White, A. H. *Aust. J. Chem.* **1984**, *37*, 1453.

739.75): C 66.57%, H 6.54%, N 1.89%, Y 12.02%. Found: C 65.74%, H 6.4%, N 1.76%, Y 12.18%. IR (Nujol, 2300−400 cm^{-1}) 2306 (w), 2278 (w), 1593 (s), 1564 (s), 1539 (s), 1515 (s), 1509 (s), 1453 (s), 1410 (s), 1388 (s), 1357 (m), 1287 (m), 1237 (m), 1178 (m), 1163 (m), 1091 (m), 1028 (m), 956 (m), 847 (m), 807 (w), 769 (s), 706 (s), 652 (m), 583 (w), 530 (m), 479 (m), 442 (w), 401(m). ^{1}H NMR (acetone-d_6, δ in ppm) 1.97 (s, 27H), 2.02 (s, 3H, CH_3 CN), 6.40 (s, 3H), 7.35−7.43 (m, 9H), 7.96−8.00 (m, 6H). ^{13}C NMR (acetone-d_6, δ in ppm) 0.8 (CH_3, CH_3 CN), 28.5 (CH_3, ^{t}Bu), 41.2 ($C(CH_3)_3$), 93.1 (*C*H), 117.2 (*C*N), 127.8 (Ph, C_{para}), 128.5 (Ph, C_{meta}), 131.0 (Ph, C_{ortho}), 141.0 (Ph, C_{ipso}), 183.5 (PhC−O), 201.3 (^{t}BuCO).

To obtain the solvent-free compound, the acetonitrile adduct was heated under vacuum (10^{-2} atm) at 100 °C for several hours. Anal. Calcd for $YC_{36}H_{45}O_6$ (MG 698.69): C 67.04%, H 6.49%, Y 12.72%. Found: C 66.44%, H 4.77%, Y 12.89%. IR (Nujol, range 1700−400 cm^{-1}) 1594 (s), 1562 (s), 1516 (s), 1505 (s), 1483 (s), 1453 (s), 1411 (s), 1389 (m), 1360 (m), 1290 (m), 1237 (m), 1183 (w), 1157 (w), 1144 (w), 1092 (m), 1077 (m), 1029 (w), 947 (w), 926 (w), 847 (w), 809 (w), 766 (s), 698 (s), 651 (w), 582 (w), 526 (w), 478 (w), 444 (w), 401(m). ^{1}H NMR (acetone-d_6, δ in ppm) 1.21 (s, 27 H), 6.41 (s, 3 H), 7.35−7.42 (m, 9 H), 7.97−8.00 (m, 6 H). ^{13}C NMR (acetone-d_6, δ in ppm) 28.5 (CH_3, ^{t}Bu), 41.4 ($C(CH_3)_3$), 93.3 (*C*H), 128.0 (Ph, C_{para}), 128.8 (Ph, C_{meta}), 131.2 (Ph, C_{ortho}), 141.2 (Ph, C_{ipso}), 183.7 (PhC−O), 201.5 (^{t}BuCO).

X-ray Measurements and Structure Determination of $Y(bpm)_3{\cdot}CH_3CN$. A single crystal of $Y(bpm)_3{\cdot}CH_3CN$ was mounted on a glass fiber in inert oil and transferred to the cold gas stream of a Siemens R3m/v four-circle diffractometer equipped with a LT-1 low-temperature unit. Data were collected at −140 °C in the ω-scan mode using monochromated Mo Kα radiation (λ = 0.710 73 Å). The unit cell was determined and refined from 48 reflections in the 2θ range 15−25°. Intensity data were collected and corrected for Lorentz and polarization effects, but not for absorption. Three reflections were monitored periodically every 97 reflections, without observing a systematic decrease in intensity. The number of reflections applicable to structure solution and refinement was restricted to 7300. The structure was solved by direct methods, from which the non-hydrogen atoms were located. Anisotropic refinement was applied for all non-hydrogen atoms except those of the disordered *tert*-butyl group. The H atoms were generated geometrically (C−H bonds fixed at 0.96 Å). The isotropic temperature factor of U = 0.08 Å^2 was assigned to all H atoms. Computations were performed using the SHELXTL PLUS program package on a 486 IBM PC.

CBE Experiments. The CBE machine is equipped with effusion cells, a substrate heater, a Leybold IC4 quartz crystal microbalance, a shutterable source of atomic oxygen (RF plasma source)[29] based on the MPD 21 model of Oxford Applied Research (OAR), an OAR 30 kV RHEED gun equipped with oxygen-resistant filaments, and a Hiden 2000 quadrupole mass spectrometer. The deposition system (Riber) is pumped by a 350 L/s turbomolecular pump and a 400 L/s ion pump and is equipped with a small cryopanel. The background pressure of this (unbaked) system is 1 × 10^{-9} Torr. The structural properties of the as-grown thin films were analyzed using a θ−2θ Siemens D500 X-ray diffraction system.

Results and Discussion

Precursor Synthesis and Characterization. The ligand benzoylpivaloylmethane (Hbpm) was first synthesized by Vorländer and Kalkow in 1898.[30] From UV, IR, and ^{1}H NMR spectroscopy[32−34] it was concluded that the diketone exists mainly as PhCOCH═(OH)CMe_3 (Ph, phenyl; Me, methyl). Up to now, only benzoylpivaloylmethanide complexes with alkaline earth and transition metals have been described in the literature.[35] Following the preparation method described by Sievers et al. for the $Ln(thd)_3$ complexes,[36] $Y(bpm)_3$ is obtained as the monohydrate, which tends to form an oil. The compound is very soluble in most organic solvents including pentane, but purification is quite difficult in this case. Recrystallization from acetonitrile, however, yields a crystalline acetonitrile adduct, which is much easier to purify. As the solvent can be removed by heating the complex at 100 °C under vacuum, $Y(bpm)_3{\cdot}CH_3CN$ is a *convenient storage form* for the precursor. Most of the ex and in situ studies were performed using $Y(bpm)_3{\cdot}CH_3CN$. No deterioration of the acetonitrile adduct was noticed after storage under ambient-conditions atmosphere for 2−3 months. The addition of acetonitrile prevents the formation of water complexes and allows isolation of the material in pure, crystalline form. The advantage of using anhydrous β-diketonate complexes as precursor compounds has been proven by thermogravimetric studies which showed that the dehydration of acetylacetonate, benzoylacetonate, and dibenzoylmethanide H_2O adducts of the lighter lanthanides is accompanied by hydrolysis and decomposition.[2] After the removal of CH_3 CN, $Y(bpm)_3$ can be sublimed without residue at 170 °C/10^{-4} Torr.

Table 1. Bond Lengths (Å)

Y(1)−O(1)	2.243 (5)	Y(1)−O(2)	2.263 (6)
Y(1)−O(3)	2.247 (5)	Y(1)−O(4)	2.279 (6)
Y(1)−O(5)	2.269 (6)	Y(1)−O(6)	2.281 (6)
Y(1)−N(1)	2.541 (7)	O(1)−C(3)	1.262 (9)
O(2)−C(1)	1.281 (9)	O(3)−C(16)	1.253 (9)
O(4)−C(14)	1.278 (8)	O(5)−C(29)	1.267 (10)
O(6)−C(27)	1.269 (10)	N(1)−C(40)	1.147 (10)
C(1)−C(2)	1.368 (11)	C(1)−C(8)	1.504 (11)
C(2)−C(3)	1.414 (12)	C(3)−C(4)	1.546 (12)
C(4)−C(5)	1.455 (14)	C(4)−C(6)	1.505 (14)
C(4)−C(7)	1.470 (15)	C(8)−C(9)	1.395 (12)
C(8)−C(13)	1.380 (11)	C(9)−C(10)	1.396 (13)
C(10)−C(11)	1.355 (13)	C(11)−C(12)	1.362 (13)
C(12)−C(13)	1.383 (13)	C(14)−C(15)	1.405 (10)
C(14)−C(21)	1.492 (11)	C(15)−C(16)	1.409 (11)
C(16)−C(17)	1.548 (10)	C(17)−C(18)	1.550 (13)
C(17)−C(19)	1.515 (12)	C(17)−C(20)	1.525 (11)
C(21)−C(22)	1.400 (11)	C(21)−C(26)	1.382 (10)
C(22)−C(23)	1.389 (13)	C(23)−C(24)	1.374 (12)
C(24)−C(25)	1.391 (13)	C(25)−C(26)	1.402 (13)
C(27)−C(28)	1.386 (10)	C(27)−C(34)	1.531 (10)
C(28)−C(29)	1.404 (10)	C(29)−C(30)	1.537 (10)
C(30)−C(31)	1.551 (12)	C(30)−C(32)	1.531 (12)
C(30)−C(33)	1.531 (12)	C(34)−C(35)	1.381 (11)
C(34)−C(39)	1.369 (12)	C(35)−C(36)	1.402 (11)
C(36)−C(37)	1.375 (13)	C(37)−C(38)	1.367 (13)
C(38)−C(39)	1.400 (11)	C(40)−C(41)	1.449 (11)

Crystal Structure of $Y(bpm)_3{\cdot}CH_3CN$. Details of crystal parameters, data collection, and structure refinement are given at the end of the paper. Selected bond lengths and angles are listed in Tables 1 and 2. The atomic coordinates are shown in Table 3. A view of the independent molecule is given in Figure 1. Of all the benzoylpivaloylmethanide coordination compounds, only $Cu(bpm)_2$ has been characterized by an X-ray crystal structure analysis.[38] $Y(bpm)_3{\cdot}CH_3CN$

(32) Iimura, F. *Nippon Kagaku Zasshi* **1957**, *78*, 50.
(33) Kwiatkowski, E.; Peplinski, Z. *Transition Met. Chem.* **1978**, *3*, 305.
(34) Emsley, J. *Struct. Bonding* **1984**, *57*, 147.
(35) (a) Hammond, G. S.; Nonhebel, D. C.; Wu, C.-H. S. *Inorg. Chem.* **1963**, *2*, 73. (b) Kwiatkowski, E.; Novicki, W. *Transition Met. Chem.* **1987**, *12*, 546. (c) Kwiatkowski, E.; Novicki, W.; Szyncel, M. *Thermochim. Acta* **1994**, *232*, 271.
(36) Eisentraut, K. J.; Sievers, R. E. *Inorg. Synth.* **1965**, *11*, 94.
(37) (a) Ismail, M.; Lyle, S. J.; Newbery, J. E. *J. Inorg. Nucl. Chem.* **1969**, *31*, 1715. (b) Acosta, J. J. C.; Berg, E. W. *Anal. Chim.* **1968** *40*, 101. (c) Khalmurzaev, N. K.; Murav′eva, I. A.; Martynenko, L. I.; Spytsin, V. I.; Byrke, A. I. *Russ. J. Inorg. Chem.* **1975**, *20*, 1148.

Table 2. Bond Angles (deg)

O(1)−Y(1)−O(2)	74.2(2)	O(1)−Y(1)−O(3)	78.0(2)
O(2)−Y(1)−O(3)	123.0(2)	O(1)−Y(1)−O(4)	125.6(2)
O(2)−Y(1)−O(4)	82.7(2)	O(3)−Y(1)−O(4)	74.8(2)
O(1)−Y(1)−O(5)	81.4(2)	O(2)−Y(1)−O(5)	103.9(2)
O(3)−Y(1)−O(5)	119.8(2)	O(4)−Y(1)−O(5)	152.8(2)
O(1)−Y(1)−O(6)	129.2(2)	O(2)−Y(1)−O(6)	154.5(2)
O(3)−Y(1)−O(6)	77.0(2)	O(4)−Y(1)−O(6)	88.7(2)
O(5)−Y(1)−O(6)	74.1(2)	O(1)−Y(1)−N(1)	138.5(2)
O(2)−Y(1)−N(1)	77.0(2)	O(3)−Y(1)−N(1)	143.5(2)
O(4)−Y(1)−N(1)	78.6(2)	O(5)−Y(1)−N(1)	77.3(2)
O(6)−Y(1)−N(1)	77.8(2)	Y(1)−O(1)−C(3)	138.1(5)
Y(1)−O(2)−C(1)	135.7(5)	Y(1)−O(3)−C(16)	133.7(5)
Y(1)−O(4)−C(14)	133.6(5)	Y(1)−O(5)−C(29)	137.1(5)
Y(1)−O(6)−C(27)	135.7(5)	Y(1)−N(1)−C(40)	169.1(7)
O(2)−C(1)−C(2)	124.8(7)	O(2)−C(1)−C(8)	114.8(7)
C(2)−C(1)−C(8)	120.4(7)	C(1)−C(2)−C(3)	124.1(7)
O(1)−C(3)−C(2)	122.8(7)	O(1)−C(3)−C(4)	116.6(7)
C(2)−C(3)−C(4)	120.6(7)	C(3)−C(4)−C(5)	115.3(8)
C(3)−C(4)−C(6)	107.5(9)	C(5)−C(4)−C(6)	108.4(9)
C(3)−C(4)−C(7)	111.8(8)	C(5)−C(4)−C(7)	109.4(9)
C(6)−C(4)−C(7)	103.8(8)	C(1)−C(8)−C(9)	123.6(7)
C(1)−C(8)−C(13)	118.2(7)	C(9)−C(8)−C(13)	118.1(8)
C(8)−C(9)−C(10)	120.1(8)	C(9)−C(10)−C(11)	119.9(8)
C(10)−C(11)−C(12)	121.1(9)	C(11)−C(12)−C(13)	119.6(8)
C(8)−C(13)−C(12)	121.2(8)	O(4)−C(14)−C(15)	125.3(7)
O(4)−C(14)−C(21)	115.1(6)	C(15)−C(14)−C(21)	119.5(6)
C(14)−C(15)−C(16)	122.3(6)	O(3)−C(16)−C(15)	124.7(7)
O(3)−C(16)−C(17)	114.4(7)	C(15)−C(16)−C(17)	120.9(6)
C(16)−C(17)−C(18)	106.2(6)	C(16)−C(17)−C(19)	107.0(7)
C(18)−C(17)−C(19)	110.0(8)	C(16)−C(17)−C(20)	114.5(7)
C(18)−C(17)−C(20)	107.9(7)	C(19)−C(17)−C(20)	111.1(7)
C(14)−C(21)−C(22)	121.9(7)	C(14)−C(21)−C(26)	119.0(7)
C(22)−C(21)−C(26)	119.1(8)	C(21)−C(22)−C(23)	120.7(7)
C(22)−C(23)−C(24)	119.5(8)	C(23)−C(24)−C(25)	121.1(9)
C(24)−C(25)−C(26)	119.0(8)	C(21)−C(16)−C(25)	120.6(7)
O(6)−C(27)−C(28)	124.9(7)	O(6)−C(27)−C(34)	114.8(6)
C(28)−C(27)−C(34)	120.3(7)	C(27)−C(28)−C(29)	123.7(7)
O(5)−C(29)−C(28)	123.7(7)	O(5)−C(29)−C(30)	114.5(6)
C(28)−C(29)−C(30)	121.7(7)	C(29)−C(30)−C(31)	108.2(6)
C(29)−C(30)−C(32)	114.6(6)	C(31)−C(30)−C(32)	109.3(8)
C(29)−C(30)−C(33)	106.8(7)	C(31)−C(30)−C(33)	107.7(7)
C(32)−C(30)−C(33)	110.0(7)	C(27)−C(34)−C(35)	117.7(7)
C(27)−C(34)−C(39)	122.2(7)	C(35)−C(34)−C(39)	120.0(7)
C(34)−C(35)−C(36)	119.8(8)	C(35)−C(36)−C(37)	119.9(8)
C(36)−C(37)−C(38)	119.9(7)	C(37)−C(38)−C(39)	120.5(9)
C(34)−C(39)−C(38)	119.8(8)	N(1)−C(40)−C(41)	179.4(9)

Table 3. Atomic Coordinates ($\times 10^4$) and Equivalent Isotropic Displacement Coefficients ($Å^2 \times 10^3$)

	x	y	z	U (eq)[a]
Y(1)	401(1)	572(1)	7422(1)	15(1)
O(1)	1013(6)	−542(4)	8455(3)	24(1)
O(2)	1022(6)	−996(4)	6855(3)	27(1)
O(3)	1864(6)	1751(4)	8293(3)	25(1)
O(4)	1842(5)	1428(4)	6655(3)	24(1)
O(5)	−1709(6)	41(4)	7703(3)	25(1)
O(6)	−696(6)	2159(4)	7414(3)	28(1)
N(1)	−1081(7)	408(6)	6025(4)	34(1)
C(1)	1367(8)	−1941(6)	7108(5)	22(1)
C(2)	1542(8)	−2221(6)	7903(5)	28(1)
C(3)	1353(8)	−1503(6)	8553(5)	25(1)
C(4)	1600(9)	−1883(7)	9436(5)	34(1)
C(5)	1394(11)	−3084(9)	9522(8)	86(2)
C(6)	3054(12)	−1486(11)	9802(10)	145(2)
C(7)	783(11)	−1311(9)	9949(7)	85(2)
C(8)	1540(8)	−2777(6)	6452(5)	24(1)
C(9)	2218(9)	−3735(7)	6601(6)	46(1)
C(10)	2279(10)	−4498(7)	5963(6)	49(1)
C(11)	1645(9)	−4322(7)	5203(6)	44(1)
C(12)	978(9)	−3393(8)	5024(6)	46(1)
C(13)	932(8)	−2620(7)	5666(5)	32(1)
C(14)	2705(8)	2296(6)	6774(5)	20(1)
C(15)	3050(8)	2953(6)	7502(4)	21(1)
C(16)	2559(8)	2651(6)	8216(5)	20(1)
C(17)	2836(8)	3452(6)	8982(5)	26(1)
C(18)	1426(9)	3804(8)	9112(6)	55(1)
C(19)	3434(11)	2786(8)	9685(6)	86(1)
C(20)	3763(9)	4511(7)	8910(5)	40(1)
C(21)	3316(7)	2635(6)	6051(5)	17(1)
C(22)	4637(8)	3178(7)	6127(5)	32(1)
C(23)	5182(10)	3485(8)	5444(5)	48(1)
C(24)	4402(10)	3273(7)	4687(6)	48(1)
C(25)	3086(10)	2734(7)	4592(5)	47(1)
C(26)	2556(8)	2405(6)	5284(5)	28(1)
C(27)	−1831(8)	2415(6)	7581(4)	19(1)
C(28)	−2886(8)	1654(6)	7722(5)	22(1)
C(29)	−2793(7)	497(6)	7752(4)	18(1)
C(30)	−4048(8)	−328(6)	7795(5)	25(1)
C(31)	−3629(9)	−1173(7)	8450(6)	49(1)
C(32)	−5296(8)	218(7)	7986(7)	49(1)
C(33)	−4405(10)	−977(8)	6972(6)	58(1)
C(34)	−1997(8)	3669(6)	7598(4)	22(1)
C(35)	−1193(8)	4343(6)	7174(5)	28(1)
C(36)	−1306(9)	5498(7)	7174(6)	37(1)
C(37)	−2180(9)	5960(6)	7618(6)	38(1)
C(38)	−2962(9)	5289(7)	8043(5)	38(1)
C(39)	−2866(8)	4134(6)	8039(5)	30(1)
C(40)	−1907(9)	391(7)	5457(5)	30(1)
C(41)	−2956(9)	379(7)	4743(5)	36(1)

[a] Equivalent isotropic U is defined as one-third of the trace of the orthogonalized U_{ij} tensor.

crystallizes in the triclinic space group $P\bar{1}$ with two molecules per unit cell. The yttrium atom is coordinated by six oxygen atoms in a distorted trigonal prismatic array, with the nitrogen atom N1 of the acetonitrile molecule capping one face of the prism formed by O2, O4, O5, and O6. The Y−O bond lengths range from 2.243(5) to 2.281(5) Å; the Y−N distance is 2.551(7) Å. The C−O bond distances and the C−C distances compare well with the values found in the H_2O adducts of yttrium benzoylacetonate,[39] $Y(bzac)_3 \cdot H_2O$, and yttrium tetramethylheptanedionate,[40] $Y(thd)_3 \cdot H_2O$.

Thermal Analysis. Combined TGA/DTA studies have been performed under an oxygen and nitrogen atmosphere to obtain information about the thermal stability, the reactivity with oxygen and the decomposition behavior. To avoid partial sublimation, closed alumina crucibles containing $Y(bpm)_3 \cdot CH_3CN$ samples of about 25 mg were used. The two curves in Figure 2 represent the weight loss (TGA) and the DTA of the compound heated under oxygen. The first mass loss of 5−6% between 87 and 112 °C corresponds to the loss of the acetonitrile molecule and is connected with a small endothermic peak. The second endothermic peak in the DTA occurs at the melting point (184 °C). Decomposition sets in at about 180 °C, presumably with the opening of a chelate ring, followed by a slow decomposition/polymerization process characterized by two not very distinct steps in the TGA. Whereas the first step is not accompanied by large enthalpy changes, the final conversion to Y_2O_3, complete at about 500 °C, is a very exothermic process. The total mass loss is slightly smaller than expected: only 82.55% instead of 84.71%. This means that the oxide, verified to be yttrium oxide by X-ray diffraction, is probably contaminated by an initial off-stoichiometric composition.

As the oxygen background pressure in the CBE system under the deposition conditions is very low (10^{-5} Torr), the thermal analysis under nitrogen accounts better for the situation of the precursor in the effusion cell.

(38) Baidina, I. A.; Stabnikov, P. A.; Igumenov, I. K.; Borisov, S. V. *Russ. J. Coord. Chem.* **1989**, *15*, 461.
(39) Cotton, F. A.; Legzdins, P. *Inorg. Chem.* **1968**, *7*, 1777.
(40) Gleizes, A.; Sans-Lenain, S.; Medus, D.; Hovnanian, N.; Miele, P.; Foulon, J.-D. *Inorg. Chim. Acta* **1993**, *209*, 47.

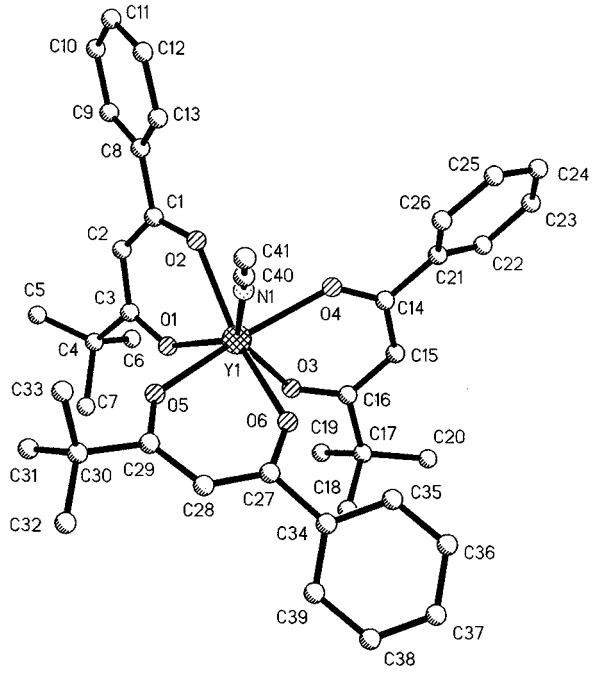

Figure 1. Structure of the $Y(bpm)_3 \cdot CH_3CN$ molecule.

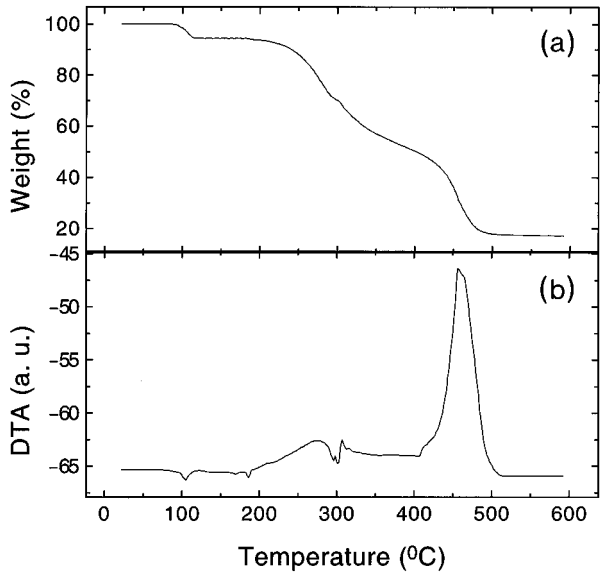

Figure 2. (a) TGA and (b) DTA of $Y(bpm)_3 \cdot CH_3CN$ under O_2.

The TGA/DTA curves differ considerably from the measurements performed under oxygen in the higher temperature range (Figure 3). The enthalpy changes in the DTA, recorded with a higher sensitivity than in the measurement under oxygen, are comparatively small and mostly endothermic. The first endothermic peaks again correspond to the loss of acetonitrile between 84 and 108 °C and the melting point at 184 °C. A small peak around 200 °C may be due to some internal rearrangement or another phase transition. Decomposition sets in at 250 °C and is not finished until 600 °C. It takes place in two steps, at 260−440 and 440−600 °C. In contrast to the behavior under oxygen, the final step is connected with an increasingly endothermic reaction. The total mass loss is much smaller than the theoretical one (79% versus 84%) owing to carbonaceous residues in the decomposition product.

The thermal analysis suggests that $Y(bpm)_3$ should be thermally stable in the CBE apparatus up to an evaporation temperature of ≃250 °C and may easily be converted into crystalline yttria at temperatures as low as 500 °C/10^{-8} Torr under molecular oxygen.

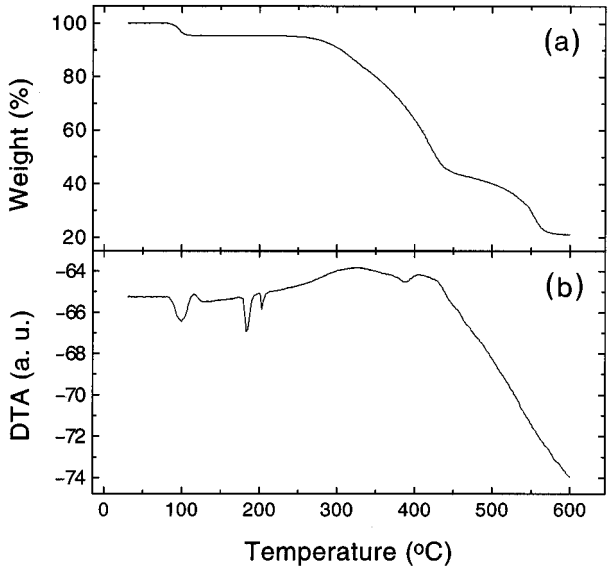

Figure 3. (a) TGA and (b) DTA of $Y(bpm)_3 \cdot CH_3CN$ under N_2.

Table 4. Peak Position (in amu) and Relative Intensities Obtained from EI and CI of $Y(bpm)_3$

species	mass	intensity	mass	intensity
$Y(bpm)_3$	698	28	699	34
$Y(bpm)_3-{}^tBu$	641	41		
$Y(bpm)_2$	495	100		
$Y(bpm)_2-Me$	480	8		
$Y(bpm)_2-2Me$	465	5		
Y(bpm)	292	8		
H(bpm)	204	2	205	100
$H_2bpm-20$			185	23
$H(bpm)-{}^tBu$	147	12	147	5
PhCO	105	5		

Mass Spectroscopic Studies. The ex situ electron ionization (EI) and chemical ionization mass spectra (CI MS) of $Y(bpm)_3$ and $Y(bpm)_3 \cdot CH_3CN$ reveal that the acetonitrile molecule is lost very easily, as the highest peak in both spectra corresponds to the $Y(bpm)_3$ molecule. The major peak in the EI spectra—taken at 70 eV—corresponds to $Y(bpm)_2$, but its absence in the CI spectra indicates that it is due to electron-induced fragmentation. However, on the time scale of the experimental temperature ramps (1 °C/s) used here, slow decomposition processes cannot be identified. The major peaks in the CI MS appear at 699 and 205 amu. The chemical ionization process occurs on a smaller energy scale than the electron ionization does and uses protons as the ionizing species. The protonation of the anionic ligand probably favors the complete decomposition of the complex into yttrium and Hbpm without an $Y(bpm)_2$ intermediate.

Table 4 lists the main peaks and their relative intensities obtained from ex situ CI MS and EI at 70 eV MS, respectively. For the sake of clarity, we have omitted the peaks due to isotopes of the main yttrium mass and those due the masses below 100 amu.

In Situ Measurements. *Evaporation Rate.* Prior to the in situ studies, the acetonitrile adduct was thoroughly degassed at 130 °C for 2 days in the CBE system. To study the sublimation behavior of the degassed yttrium complex, we measured the evaporation rate as a function of temperature, using a quartz

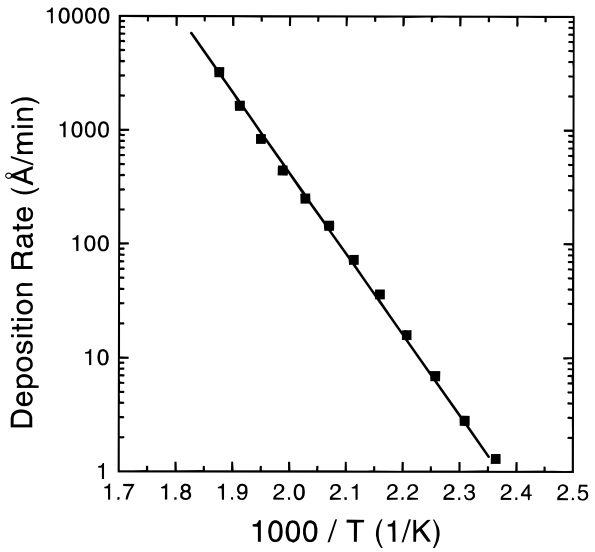

Figure 4. Evaporation rate of $Y(bpm)_3$ versus temperature.

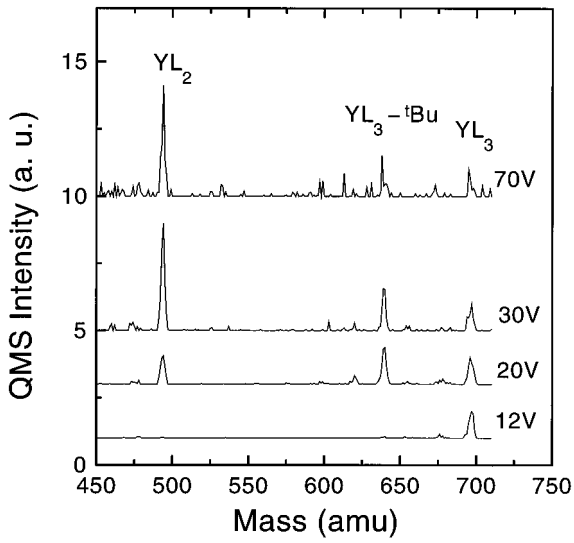

Figure 5. Mass spectra of the effusive beam for different electron ionization values.

crystal monitor set with a tooling factor of 100%, a density of 1.00, and a *Z* factor of 1.00. In Figure 4 the deposition rate is plotted against the evaporation temperature. Even at very high evaporation rates (1200 Å), the pressure does not rise significantly, satisfying almost perfectly the first condition for an "ideal" precursor given above.

Beam Composition. The in situ mass spectrometric studies have been performed to answer the following *crucial* questions: (1) Which metal-containing volatile species are present in the beam (YL_3, YL_2, L: ligand) coming out of the effusion cell; (2) does their relative ratio change as a function of deposition conditions (time, temperature, pressure); (3) are the precursor and the evaporation rates stable under the vacuum and deposition conditions (≃200 °C and $1-5 \times 10^{-5}$ Torr O_2)? While for the ex situ mass spectroscopic experiments a small quantity of the sample is vaporized with a high heating rate (1 °C/s), the in situ experiments can be performed closer to equilibrium conditions (i.e., at constant temperature over a long time interval). This allows the detection of slow decomposition processes.

To determine the composition of the effusive beam at the evaporation temperature used for thin film growth (200 °C, corresponding to a deposition rate of ≃140 Å/min), electron ionization mass spectra have been recorded at 70, 30, 20, and 12 eV. The various intensities have—in each spectrum—been scaled versus the intensity of the YL_3 peak. As can be seen in Figure 5, with a reduced ionization energy, we observe that the relative intensity of the various fragments decreases, proving that a significant intensity of masses different from YL_3 is indeed due to ionizer fragmentation. Hence, the effusive beam consists essentially of monomeric YL_3, fulfilling our second requirement for an "ideal" precursor, namely, the presence of a single metal-containing species in the molecular beam.

In an further attempt to determine in which temperature range the precursor is stable, we studied the evolution of the major yttrium-containing peaks at an ionization energy of 15 eV (YL_3, $YL_3-{}^tBu$, and YL_2) as the temperature and evaporation rate are increased. Figure 6 shows that even at temperatures as high as 260 °C (corresponding to a deposition rate of 1200 Å/min) the peak intensities of $YL_3-{}^tBu$ and YL_2 are at least 2 orders of magnitude lower than the intensity of

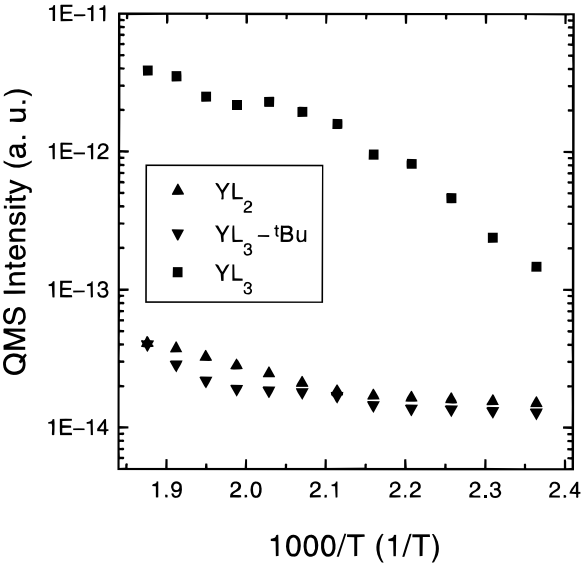

Figure 6. Evolution of YL_3, $YL_3-{}^tBu$, and YL_2 peak intensities as a function of evaporation rate, measured using an ionization energy of 15 eV.

the molecular peak. This indicates a remarkable *stability of the precursor in a wide temperature range.*

To determine whether the precursor sticks well on the surface and shutter walls, the evolution of YL_2, YL_3, and L, measured using an ionization energy of 70 eV, is recorded during a shuttering experiment performed at a temperature of 210 °C and an evaporation rate of 100 Å/min. At the outset of this experiment, the shutter of the corresponding effusion cell is closed, and only a signal from L is detected in the background, as seen in Figure 7. As this experiment was performed with precursor material prepared using the original method,[36] a possible ligand-induced contamination could be the reason for the presence of L, or perhaps there is a faint decomposition process. Hence, L is volatile under these conditions and *has a low sticking coefficient* (the quartz monitor registers no deposition of material). On the other hand, the absence of the YL_2 and YL_3 peaks convincingly suggests that *these molecules stick well on the shutter and chamber walls.* After opening the shutter, the intensities of these latter peaks as well as that of HL increase and reach an equilibrium value. The

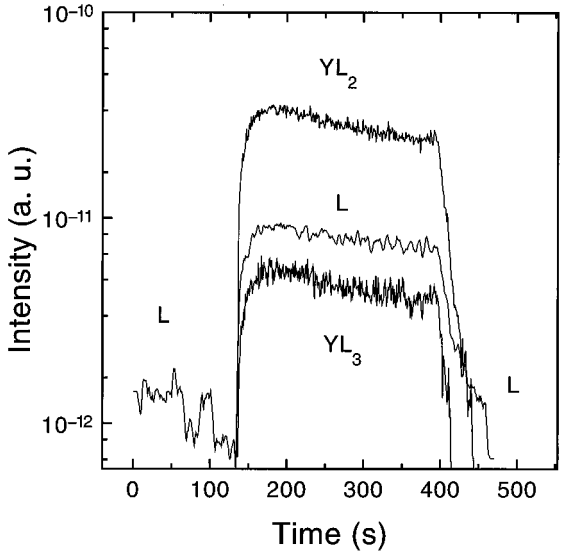

Figure 7. Evolution of the L, YL_2 and YL_3 peak intensities as a function of time during a shuttering cycle, measured using an ionization energy of 70 eV.

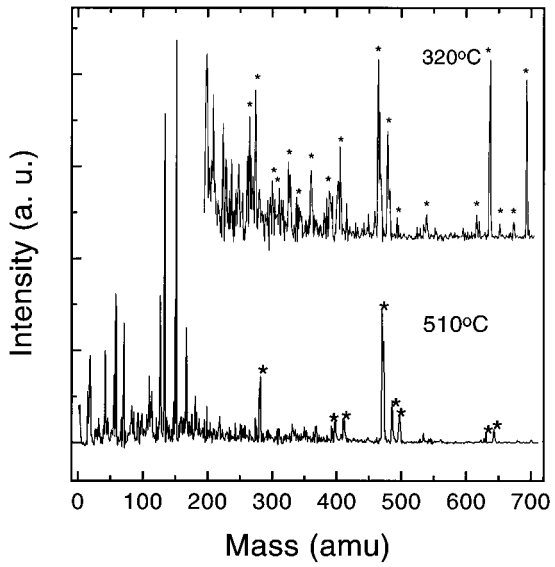

Figure 8. Decomposition spectra of $Y(bpm)_3$ for substrate temperatures of 320 and 510 °C.

Table 5. Peak in Mass Spectrum of Direct Beam after Impingement upon a Heated MgO Substrate

mass	species
57	^{t}Bu
70	(bpm)−Ph−^{t}Bu(=$C_3H_2O_2$)
77	Ph
126	(bpm)−Ph
132	(bpm)−^{t}Bu−CH_3(=PhC(O)$CHCH_2$)
146	(bpm)−^{t}Bu
162	$PhC(O)CH_2C(O)CH_3$
216	Y(bpm)−Ph
278	Y(bpm)−CH_3
390	$Y(bpm)_2$−PhCO
410	$Y(bpm)_2$−^{t}BuCO
465	$Y(bpm)_2$−$2CH_3$
480	$Y(bpm)_2$−CH_3
495	$Y(bpm)_2$
530	$Y(bpm)_3$−$2PhCH_3$
622	$Y(bpm)_3$−Ph
642	$Y(bpm)_3$−^{t}Bu

slow decrease is due to a lowering of the temperature in the cell caused by the opening of the shutter (and the corresponding loss of thermal radiation).

A growth experiment for the preparation of a film with a thickness of 500−1000 Å typically takes between 2 and 4 h of deposition. To determine the long-term stability of the precursor, the temperature of the effusion cell was set to 220 °C, and the evaporation rate was measured using the quartz monitor. The initial rate was 190 Å, but this value dropped to about 160 Å over a time interval of about 3 h, i.e., a change of about 4% per hour, mainly due to a change in effusion-cell filling. Taking the measured drift into account, this stability is sufficient to prepare oxide thin films using the *block-by-block*[41] or a *monolayer-by-monolayer* deposition method.

Because the deposition of the oxide films takes place under a molecular oxygen background pressure of 1−3 × 10^{-5} Torr, the earlier experiments were repeated to check whether specific reactions with molecular oxygen occur. Under varying oxidation conditions, however, the signals obtained from a mass spectrometer tend to

Table 6. Structure Determination Summary

Crystal Data	
empirical formula	$C_{41}H_{48}NO_6Y$
color, habit	colorless, prism
crystal size (mm)	0.5 × 0.5 × 0.45
crystal system	triclinic
space group	$P\bar{1}$
unit-cell dimensions	a = 9.961(4) Å
	b = 12.020(4) Å
	c = 16.711(4) Å
	α = 91.87(2)°
	β = 99.47(2)°
	γ = 95.14(2)°
volume	1963.4(12) Å
Z	2
formula weight	739.7
density (calc.)	1.251 Mg/m^3
absorption coefficient	1.530 mm^{-1}
F(000)	776
Data Collection	
diffractometer used	Nicolet R3
radiation	Mo Kα (λ = 0.710 73 Å)
temp (K)	153
monochromator	highly oriented graphite crystal
2θ range	4.0−54.0°
scan type	ω
scan speed	variable; 4.19−29.30°/min in ω
scan range (ω)	1.20°
background measurement	stationary crystal and stationary counter at beginning and end of scan, each for 20.0% of scan time
standard reflections	3 measured every 97 reflections
index ranges	$-1 \le h \le 8$, $-15 \le k \le 15$, $-21 \le l \le 21$
reflections collected	7292
independent reflections	6837 (R_{int} = 7.28%)
observed reflections	4710 ($F > 4.0\sigma(F)$)
absorption correction	N/A
Solution and Refinement	
system used	Siemens SHELXTL PLUS (PC version)
solution	direct methods
refinement method	full-matrix least-squares
quantity minimized	$\sum w(F_o - F_c)^2$
absolute structure	N/A
extinction correction	N/A
hydrogen atoms	riding model, fixed isotropic U
weighting scheme	$w^{-1} = \sigma^2(F) + 0.0013F^2$
no. of parameters refined	422
final R indexes (obs. data)	R = 9.25%, wR = 9.75%
R indexes (all data)	R = 13.99%, wR = 17.27%
goodness of fit	1.51
largest and mean Δ/σ	0.327, 0.019
data-to-parameter ratio	11.2:1
largest difference peak	1.21 e Å^{-3}
largest difference hole	−2.25 e Å^{-3}

(41) Locquet, J.-P.; Mächler, E. *MRS Bull.* **1994**, *19*, 39.

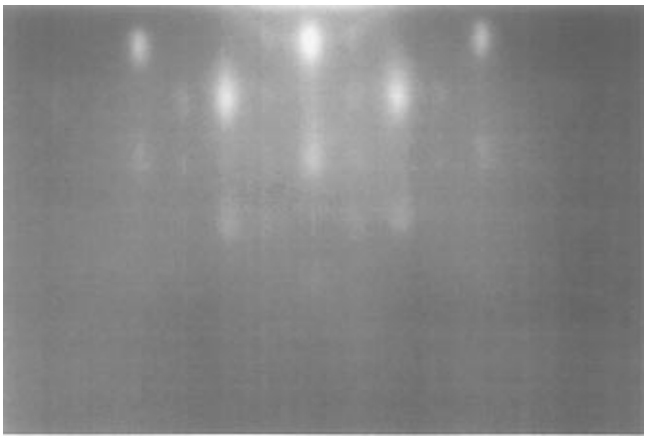

Figure 9. RHEED pattern along the [001] axis of $SrTiO_3$.

change significantly, owing to the oxygen sensitivity of various elements such as the filament and the microchannel plates. Therefore it was impossible to separate the real changes of the precursor spectra from the changes of the mass spectrometer itself. However, over the time interval used in this experiment (2−3 h), the deposition rate as measured by the quartz monitor did not change significantly, which suggests a good stability of the precursor under these conditions.

Regarding the handling of this compound, no deterioration of the precursor and the acetonitrile adduct was noticed over a period of 2−3 months under ambient conditions. The acetonitrile is toxic but can be eliminated by a simple heating process prior to the use and introduction into the CBE system. Under these conditions, the product becomes a nontoxic compound, thus fulfilling our final condition.

Beam Decomposition Studies. To obtain information about the decomposition behavior of the compound under vacuum at higher temperatures, decomposition mass spectra were recorded after impingement of the precursor beam on a heated MgO substrate (Figure 8) at an ionization voltage of 15 eV and an evaporation temperature of 180 °C. Thermal decomposition of $Y(bpm)_3$ sets in only at temperatures of more than 300 °C. The initial steps of thermal fragmentation are similar to ionization-induced fragmentation (loss of *tert*-butyl groups and ligands). At a substrate temperature of 510 °C, thermal decomposition is still incomplete, with many volatile and yttrium-containing species surviving the interaction with the heated substrate. Table 5 gives a tentative assignment of the major peaks.

Film Deposition and Characterization. Finally $Y(bpm)_3$ was used to deposit yttrium oxide thin films on $SrTiO_3$. Typical growth conditions were (i) a substrate temperature of 600 °C, (ii) an evaporation rate of 30 Å/min (measured using the quartz monitor and the same settings as above), (iii) an atomic oxygen flux of $\simeq 5 \times 10^{15}$ atoms/cm^2 at 400 W of rf power, and (iv) a background O_2 pressure of 2.5×10^{-5} Torr. The total thickness of the films was typically 1 μm (quartz monitor). After the deposition the effusion cell containing the precursor was cooled to ≃100 °C, which took about 90 min, before the substrate heater was turned off.

During growth, the evolution of the crystal surface was monitored using RHEED. A typical RHEED image, obtained along the $SrTiO_3$ [100] azimuth, is shown in Figure 9. This confirms the epitaxial in-plane arrangement Y_2O_3 [110] || $SrTiO_3$ [100], as already observed for the growth of Dy_2O_3 on $SrTiO_3$.[15] The absence of vertical streaks in this image suggests that the growth is not two-dimensional. Indeed our previous studies on the growth of Dy_2O_3 show the formation of domains, having typical sizes of 10−40 nm and separated by domain boundaries parallel to the surface normal, and thus explain the observation of spots in the RHEED pattern.

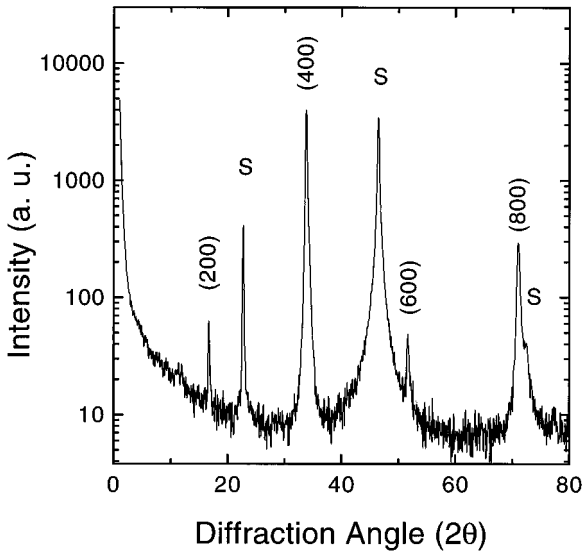

Figure 10. X-ray diffraction spectrum of the Y_2O_3 thin film.

The X-ray diffraction spectrum in Figure 10 shows only the Y_2O_3 [00*l*] (*l*: 2, 4, 6, 8) peaks, indicating the out-of-plane epitaxial arrangement Y_2O_3 [001] || $SrTiO_3$ [001]. The absence of carbonate-containing impurities suggests an efficient decomposition of the precursor under the atomic oxygen flux. The position of the Y_2O_3 [004] peak corresponds to a unit cell of 10.60 Å, in good agreement with bulk values. The absence of any other reflections in the diffraction spectrum of such a thick film confirms the epitaxial growth of this compound, despite the observation of 3D domains in the RHEED pattern. Y_2O_3 has a body-centered structure with $a = b = c = 1.06$ nm and belongs to the space group $Ia\bar{3}$. Although cubic, it has neither 4-fold symmetry axes nor mirror planes.

Conclusions

In conclusion, a novel, Y-containing metalorganic precursor has been developed for use in a low-pressure CBE environment. This precursor fully meets the conditions necessary for a precisely controlled deposition process of complex oxides. It can be sublimed as a mononuclear species without significant decomposition over a wide temperature range, sticks well on the cold parts of the system, and decomposes under atomic oxygen to yield epitaxial yttria thin films.

Acknowledgment. Support for this work from the Schweizerischer Nationalfonds zur Förderung der Wissenschaftlichen Forschung, Project No. NFP 30, is gratefully acknowledged. Special thanks are given to P. Fortunato for the help with the TGA/DTA measurements. The authors acknowledge stimulating discussions with J. G. Bednorz, J. R. Huber, and P. Felder over the past years.

CM9602510